http://journal.uir.ac.id/index.php/JGEET

E-ISSN : 2541-5794
P-ISSN : 2503-216X

Journal of Geoscience,
Engineering, Environment, and Technology
Vol 10 No 2 2025

RESEARCH ARTICLE

Characteristics of Groundwater Hydrochemistry and Stable Isotopes ($\delta^{18}O$ & $\delta^{2}H$) in Cadasari, Banten, Indonesia

Hadi Hidayat [1]*, Boy Yoseph[1], Teuku Yan Waliana Muda Iskandarsyah[1]

[1] *Faculty of Geological Engineering, Universitas Padjadjaran, Jatinangor, Sumedang, West Java, Indonesia.*

* Corresponding author: hadihidayat17@gmail.com
Tel.:+6281313984189
Received: Feb 25, 2025; Accepted: May 31, 2025.
DOI: 10.25299/jgeet.2025.10.02.21531

Abstract

Groundwater is an essential resource for drinking and domestic use, displaying significant diversity in volcanic regions.This study focuses on Cadasari, Banten, Indonesia, and aims to determine the hydrochemical characteristics of groundwater and the stable isotopes ($\delta^{18}O$ & $\delta^{2}H$). Hydrogeological mapping was employed, and analytical data were collected from 20 groundwater sources, including springs, rivers, and wells, at elevations ranging from 167 to 928 meters above sea level. The hydrochemical analysis revealed various groundwater types, such as Ca-HCO_3, Ca+Mg-HCO_3, Na+K+Ca-HCO_3, and Na+K+Ca-Cl. These variations in groundwater types are attributed to differences in volcanic lithofacies. Gibbs and Gaillardet's diagrams indicate that water-rock interaction processes primarily influence the variability of these groundwater facies in Cadasari, highlighting the significant role of silicate minerals in the groundwater's geochemistry. The isotopic composition of borehole samples shows an average isotope ratio of -7.0 ‰ for $\delta^{18}O$ and -41.7 ‰ for $\delta^{2}H$, while dug well samples have average ratios of -6.1 ‰ for $\delta^{18}O$ and -34.9 ‰ for $\delta^{2}H$. Spring samples exhibit an average isotope ratio of -6.7 ‰ for $\delta^{18}O$ and -39.3 ‰ for $\delta^{2}H$. The isotopic composition across the groundwater samples suggests that the water in this area is of meteoric origin.

Keywords: Cadasari**,** Groundwater, Hydrochemistry, stable isotope, Volcanic aquifer.

1. Introduction

Volcanic deposits, with their unique ability to act as productive aquifers and provide abundant groundwater resources, are a captivating natural phenomenon. Many places in Indonesia rely on groundwater from these aquifers. One such fascinating example is Mount Bromo-Tengger in the eastern region of Java Island (Toulier et al., 2019) In the middle part of Java Island is Mount Merapi (Hendrayana et al., 2022; Razi et al., 2024), and in the western region of Java Island is Mount Salak (Alfadli et al., 2021) and Mount Ciremai (Dianardi et al., 2018; Irawan et al., 2009). Another is Mount Karang, a volcanic mountain in the western part of Java Island, which boasts significant groundwater potential (Alam et al., 2014). Our research area, situated in Cadasari on the eastern slopes of Mount Karang, is not just a site for study but a pivotal location where groundwater is a vital source of freshwater for drinking and other domestic purposes. Due to problems with clean water in Cadasari, five villages experience a clean water crisis every year, including Koranji Village, Kaduela, Kaduengang, Pasir Peutuey, and Kurung Dahu (Bingar, 2024; Mardiana, 2024). This underscores the importance of rational utilisation and sustainable management of these unique groundwater resources (Liu et al., 2019) What sets our research apart is the novel focus on the hydrochemical characteristics and stable isotopes ($\delta^{18}O$ and $\delta^{2}H$) to determine the groundwater origin. There are several studies regarding the hydrochemical characteristics of volcanic aquifers and stable isotope studies to determine the origin of groundwater, including (Maria et al., 2021; Toulier et al., 2019). The expected output from this study's results can be used as a reference in determining strategies to maintain sustainable groundwater use.

2. Study Area

2.1 Location

This research was carried out on Cadasari, Pandeglang, Banten, Indonesia (Figure 1), which is geographically located at 106˚ 3`28" E 6˚ 13`18" S and 106˚ 8`39" E 6˚ 17`51" S.

The research area is located on the morphology of the mountain's slopes and solitary hills at its foot, with slopes ranging from sloping to steep. The river's morphology follows the shape of a volcano. It has steep gradients, narrow valleys on the upper slopes, and a radial flow pattern, with water flowing from west to east.

The study area's average annual rainfall is about 1323 mm. This area has a dry season month under the Köppen climate classification for tropical climates (Kottek et al., 2006). August and September have average monthly rainfall of less than 60 mm, and the average annual temperature is 27.1˚C. The underlying hydrogeological setting of the study area was formed during the Quaternary Periods.

2.2 Geological and hydrogeological condition

Volcanic activity in the study area lasted from the Pleistocene to the Holocene and formed the oldest volcanoes in the area, such as Mt. Karang and Mt. Parakasak. Mt. Karang and Mt. Pulosari still have a volcanic cone shape

and a stratovolcano shape. The highest point of Karang is 1778 meters above sea level (Rusmana, 1991).

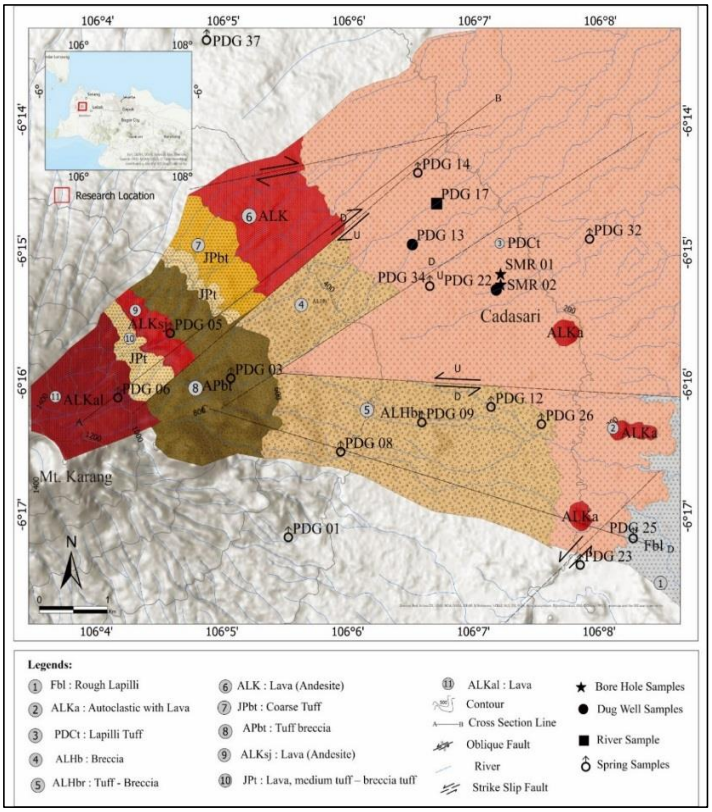

Fig 1. Show the study area, the geological condition of the study area, and the sampling locations on Cadasari on the eastern slope of Mount Karang, Banten, Indonesia

The Lithology on Cadasari is divided into 11 (eleven) volcanic lithofacies, which are interpreted as the result of 5 (five) eruptions of Karang Mountain (Figure 1), the results of the first eruption depositing the old rough lapilli rock facies (Fbl) autoclastic facies with lava (ALKa). Well-sorted lapilli tuff facies (PDct) and the grain-supported pyroclastic-breccia breccia facies (ALHb), then the second eruption produces pyroclastic breccia-tuff grain-supported facies (ALHbr), the result of the third eruption is andesite lava facies (ALK), coarse tuff facies – matrix supported graded bedding facies (JPbt) tuff breccia, poorly sorted matrix supported tuff breccia facies (APbt), fourth eruption of Karang Mountain produced andesite sheeting joint (ALKsj) lava facies, medium tuff facies – breccia tuff matrix supported graded bedding (Jpt). The fifth eruption of Mount Karang also produced auto-clastic with lava facies (ALKal).

The geological structures developed in the study area are the Cilenggor sinistral horizontal fault, the Cikirup normal fault, the Cikarang normal-dextral fault, and the Cilalaki normal-sinistral fault.

Based on the geological condition, the study area has three different aquifer systems: (1) The aquifer system in autoclastic lithology, which includes lava and andesite lava (fractured system). (2) The aquifer system in pyroclastic breccia lithology and tuff grain support (combined between contact and porus), and (3) the aquifer system in tuff and lapilli lithology (porus).

3. Methods

This study was conducted by conducting a field survey first from January to March 2020, then laboratory analysis and data interpretation were carried out, for more details it is described in the following chart (figure 2).

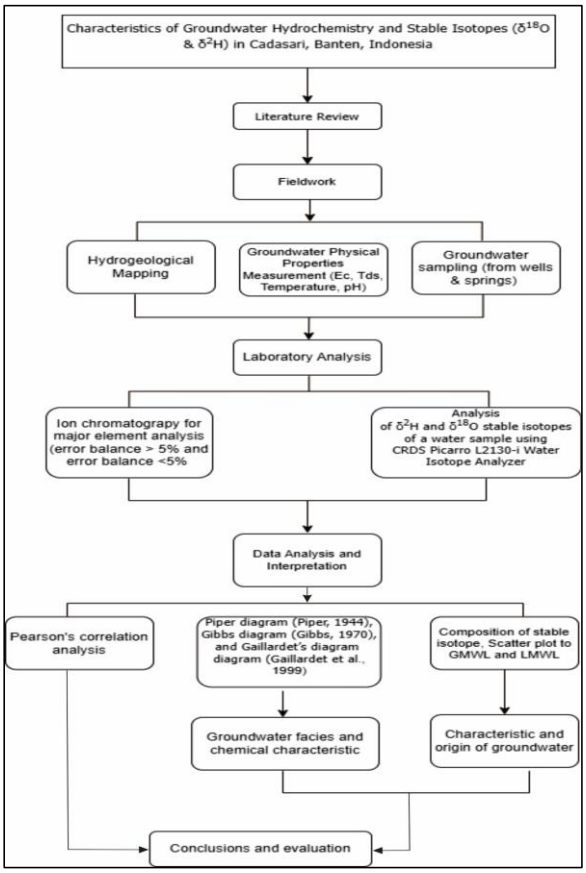

Fig 2. Research Methods Flowchart

3.1 Hydrogeological Mapping

Hydrogeological mapping is a method used during fieldwork in the Cadasari area and its surroundings, involving the exploration of groundwater sources, such as springs (Figures 3a and 3b), drilled wells (Figure 3c), and dug wells. Springs are generally in contact with volcanic lithofacies and have varying valley morphologies. Two dug wells are located at 297 m and 239 m a.s.l.

Figure 3. a.An example of a groundwater source in the form of a spring at the PDG-9 observation point in the study area. b. An example of a groundwater source in the form of a spring at the PDG-12 observation point in the study area..c.An example of a groundwater source in the form of a drilled well at the SMR-01 observation point in the study area.

3.2 Water sampling

Groundwater sampling was carried out by exploring the study area to collect groundwater samples from various hydrogeological points of interest, including 15 samples from springs, two from dug wells, one from a river, and 2 from boreholes.

Water sampling was performed using 500-mL polyethene bottles. Before sampling, the bottles, ladle, filtration units and messy inside were rinsed with filtered water three times. The water samples were filtered in situ using a 0.45 µm syringe filter. A sample of as much as 500 mL was collected for cation and anion analyses. Groundwater samples of 60 mL were used for stable isotope analysis, the most commonly used stable isotopes in hydrogeological studies are oxygen and hydrogen (Gong et al., 2021).

3.3 Hydrochemical analysis methods

pH, electrical conductivity, total dissolved solids, and temperature were measured on-site using HANNA Instruments HI9811-5. The cations (Li^+, Na^+, K^+, NH_4^+ Ca^{2+} and Mg^{2+}) and anions (Cl^-, NO_3^-, SO_4^{2-}) were determined by ion chromatography (IC - metrohm type 930 Compact) in the laboratory. HCO_3^- was analysed using the titration method with 0.1 N HCl; methyl red and bromocresol green were used as indicators. A 5% difference in the electrical balance between cations and anions is required and was obtained for all samples, suggesting high accuracy of groundwater quality determinations (Liu et al., 2023).

Hydrogeochemical data were analysed using statistical and trilinear diagram methods. statistical processing was performed using IBM SPSS Statistics 25.0. Correlation analysis between parameters was conducted based on the Pearson correlation, which allows the grouping of groundwater based on the similarity of chemical and physical properties in groundwater samples (He et al., 2023), a trilinear Piper diagram (Piper, 1944), Gibbs diagram (Gibbs, 1970), and Gaillardet's diagram (Gaillardet et al., 1999) to confirm the water-rock interaction process in groundwater.

3.4 Stable isotope analysis methods

Analysis of δ^2H and $\delta^{18}O$ stable isotopes of a water sample using CRDS Picarro L2130-i Water Isotope Analyzer. The composition of isotopes is expressed as the relative ratio (δ) against Standard Mean Ocean Water (Hamed, 2014):

$$\delta = \left(\frac{R_{Sample}}{R_{SMOW}} - 1\right).1000\ ‰ \qquad (1)$$

R_{sample} represents either the $^{18}O/^{16}O$ or the $^2H/^1H$ of the sample, in ‰, and R_{SMOW} is $^{18}O/^{16}O$ or the $^2H/^1H$ ratio of the SMOW.The linear relationship between δ^2H and $\delta^{18}O$ in meteoric waters is commonly referred to as the meteoric water line. At the global scale, the average relationships between δ^2H and $\delta^{18}O$ are expressed as the global meteoric water line (GMWL) (Craig, 1961). The isotopic composition of water in natural hydrological systems is influenced by physical variables, including air temperature, air pressure, humidity, geographical location, and altitude. (Oliveira et al., 2022). Therefore, it is necessary to define an accurate local meteoric water line (LMWL) to represent the local study area adequately (Razi et al., 2024).

4. Results and Discussion

4.1 Groundwater Physical Properties

Groundwater physical properties, such as Electrical Conductivity (EC), Total dissolved solids (TDS), pH, and Temperature, are presented in Table I. Additional information for the table: n.d. means not detected, and n.a. means not analysed. The measured Electrical Conductivity (EC) values for springs, rivers, and wells ranged from 50 to 460 µS/cm, indicating that the groundwater in the study area is freshwater. (Listiawan et al., 2024). The lowest EC for groundwater was found at the PDG 6 sampling site, which had the highest spring elevation (928 m a.s.l.), suggesting a short flow path and relatively short residence time. (Liu and Yamanaka, 2012) The total dissolved solids (TDS) ranged from 20 to 220 mg/L, the pH of the springs and wells ranged from slightly acidic to neutral (5.5-7.8), and the temperature ranged from 23 to 31 °C. The concentrations of cations and anions provide valuable insights into water quality, highlighting the dominance of specific elements.

Regarding cation abundance, the hierarchy is quite clear: Ca^{2+} emerges as the most significant, with concentrations ranging from 3.16 to 41.17 mg/L and an average of 15.62 mg/L, underscoring its critical role. Na^+ levels follow closely, ranging between 3.47 and 30.37 mg/L, with an average of 11.02 mg/L, indicating its substantial presence. Mg^{2+} and K^+ are next, with Mg^{2+} demonstrating concentrations from 0.84 to 19.37 mg/L and an average of 6.87 mg/L, while K^+ ranges from 2.76 to 13.52 mg/L, averaging 5.18 mg/L.

When examining anions, HCO_3^- stands out significantly, with concentrations ranging from 13.8 to 249.7 mg/L and an impressive average of 92.7 mg/L, highlighting its

importance. Cl^- exhibits notable levels, ranging from 0.8 to 38.3 mg/L, with an average of 5.1 mg/L, while SO_4^{2-}, although less abundant, remains significant with concentrations between 1.1 and 18.7 mg/L, averaging 4.3 mg/L. The relationships between the 20 physical properties, major ions and stable isotope were evaluated using Pearson's correlation. This correlation matrix is widely used to estimate the degree of dependency between two variables. The electrical conductivity (EC) exhibited highly significant correlations with various groundwater chemical parameters (see Table 2), including Ca^{2+}, Mg^{2+}, K^+, HCO_3^-, and SO_4^{2-}. Additionally, noteworthy correlations were observed: Ca^{2+} correlated with Mg^{2+} (0.91), Ca^{2+} with K+ (0.73), Ca^{2+} with HCO_3- (0.83), Mg^{2+} with HCO_3^- (0.89), Na+ with Cl- (0.85), and K+ with $S0_4^{2-}$ (0.86).

Table 1. Water physical properties, major ions and stable isotope (δ^2H & $\delta^{18}O$) of the research area

No	Sample Code	Type	Elevation (m.a.s.l)	EC (µS/cm)	TDS (mg/L)	Temp (°C)	pH	F^- (mg/L)	Cl^- (mg/L)	NO_3^{2-} (mg/L)	SO_4^{2-} (mg/L)	HCO_3^- (mg/L)	Na^+ (mg/L)	K^+ (mg/L)	Ca^{2+} (mg/L)	Mg^{2+} (mg/L)	$\delta^{18}O$ ‰	δ^2H ‰
1	SMR-1	Borehole	237	120	50	27,8	7,8	n.d	3,5	n.d	4,9	102,0	11,09	5,42	10,42	4,81	-7,7	-44,3
2	SMR-2	Borehole	246	160	75	27,0	6,5	0,2	1,4	2,1	1,6	96,2	9,76	4,90	13,89	6,97	-7,0	-40,6
3	PDG 13	Dug Well	297	460	220	25,9	6,3	0,1	5,7	17,5	18,7	249,7	13,3	13,5	41,2	19,4	-5,4	-29,3
4	PDG 22	Dug Well	239	160	70	26,6	6,5	0,2	2,0	3,1	1,9	89,0	9,7	4,9	14,3	6,7	-6,9	-40,4
5	PDG 17	River	238	180	80	27,4	7,4	0,2	5,8	2,0	6,6	57,2	8,4	8,1	18,1	4,2	-4,2	-19,3
6	PDG 01	Spring	459	80	20	23,0	7,6	0,2	1,7	3,1	3,1	30,1	6,2	2,9	3,2	0,9	-6,8	-39,6
7	PDG 03	Spring	645	60	20	23,0	6,5	0,1	1,6	4,0	3,0	15,0	6,1	2,8	4,0	0,8	-7,2	-41,6
8	PDG 05	Spring	800	290	140	24,9	6,9	0,1	17,9	54,6	3,8	57,2	12,6	4,0	26,2	9,3	-7,3	-43,4
9	PDG 06	Spring	928	50	20	23,6	7,2	0,1	1,2	2,5	1,8	13,8	3,5	2,9	4,9	1,3	-8,2	-47,7
10	PDG 08	Spring	437	150	70	25,0	6,8	0,2	1,7	1,5	1,3	77,7	9,9	3,3	9,9	6,5	-6,6	-38,0
11	PDG 09	Spring	344	130	60	24,8	7,0	0,2	2,5	2,6	2,8	67,7	8,7	4,6	10,0	5,2	-7,4	-43,3
12	PDG 12	Spring	263	140	60	25,9	6,4	0,2	2,6	4,3	2,7	93,0	9,1	4,9	11,3	5,0	-7,1	-41,6
13	PDG 14	Spring	251	230	110	23,3	6,5	0,2	2,2	3,1	1,4	170,0	11,2	5,0	20,5	12,5	-7,0	-41,1
14	PDG 23	Spring	199	190	80	25,2	6,5	0,2	4,2	6,3	2,6	81,8	11,4	4,9	16,8	10,7	-6,5	-38,2
15	PDG 25	Spring	180	320	150	26,5	5,5	0,1	38,3	12,9	15,4	57,4	30,4	7,9	15,4	5,5	-5,6	-33,1
16	PDG 26	Spring	231	150	70	26,3	6,6	0,2	1,8	2,2	2,2	65,6	9,8	4,7	11,6	6,2	-7,0	-41,1
17	PDG 31	Spring	180	270	130	29,6	6,4	0,2	0,8	n.d	6,3	154,2	13,7	4,5	24,5	9,0	-5,7	-32,6
18	PDG 32	Spring	167	210	90	31,0	6,4	0,2	4,6	1,3	3,7	187,1	15,5	5,5	27,7	12,2	-5,1	-30,1
19	PDG 34	Spring	309	130	50	25,4	6,1	0,1	1,4	0,8	1,2	96,6	10,2	4,3	16,0	5,2	-6,2	-36,4
20	PDG 37	Spring	324	140	60	25,5	6,6	0,1	1,3	1,8	1,1	92,0	10,1	4,6	12,7	5,1	-7,2	-42,0

Table 2. Pearson's correlation coefficient (R) between the research area's Water physical properties, major ions and stable isotope (δ^2H & $\delta^{18}O$).

	Ec	TDS	pH	Ca^{2+}	Mg^{2+}	Na^+	K^+	HCO_3^-	Cl^-	SO_4^{2-}	$\delta^{18}O$	δ^2H
Ec	1.00	0.99	-0.48	0.90	0.83	0.65	0.80	0.70	0.50	0.79	0.54	0.50
TDS		1.00	-0.47	0.89	0.83	0.64	0.78	0.69	0.49	0.77	0.50	0.47
pH			1.00	-0.37	-0.38	-0.63	-0.27	-0.32	-0.42	-0.33	-0.30	-0.20
Ca^{2+}				1.00	0.91	0.41	0.73	0.83	0.20	0.59	0.58	0.55
Mg^{2+}					1.00	0.35	0.66	0.89	0.07	0.47	0.40	0.36
Na^+						1.00	0.45	0.29	0.85	0.63	0.45	0.36
K^+							1.00	0.63	0.33	0.86	0.61	0.63
HCO_3^-								1.00	-0.12	0.42	0.43	0.40
Cl^-									1.00	0.60	0.26	0.20
SO_4^{2-}										1.00	0.53	0.53
$\delta^{18}O$											1.00	0.99
δ^2H												1.00

4.2 Groundwater Facies

A Piper diagram was used to determine the groundwater facies that formed in the study area. Based on Piper diagram analysis (Figure 4), four groundwater facies have been identified on the Cadasari: Ca-HCO_3, Ca+Mg-HCO_3, Na+K-HCO_3, and Na+K+Ca-HCO_3.

The Ca-HCO_3 facies were identified at the PDG 6 and PDG 17 sampling sites. The PDG 6 sampling location is in the auto-clastic with lava (ALKal) lithofacies and has the highest sample elevation, 928 masl. The presence of HCO3- indicates that the groundwater has been mixed with shallow groundwater as a local recharge and that groundwater circulation is pretty close (Maria et al., 2021). The dominance of Ca^{2+} cations is a result of volcanic lithological weathering. The dominant bicarbonate in groundwater is thought to originate from the interaction between meteoric water and air, mainly through the CO2 in the rain precipitation process, and is found in soil and rocks within aquifers. The mineral elements in rocks are subjected to hydrolysis by meteoric water and groundwater so that some chemical compositions release, dissolve, or are carried with the water, and some precipitate with the rock (Laratmase et al., 2024).

The Ca+Mg-HCO_3 groundwater facies predominantly occur on the Cadasari. This facies includes fifteen groundwater samples, specifically PDG 05, PDG 08, PDG 09, PDG 12, PDG 13, PDG 14, PDG 22, PDG 23, PDG 26, PDG 32, PDG 34, PDG 37, SMR 02, PDG 31, and SMR 01. It is found within various volcanic lithofacies, which consist of lava (ALKsj), tuff-breccia (ALHbr), and lapilli-tuff (PDCt), spanning elevations from 800 to 167 masl. These facies form due to prolonged interactions between groundwater and rock, allowing for water mixing from different aquifers

(Suganda et al., 2021). In contrast, field observations indicate that the groundwater experiences ion exchange processes, with Ca^{2+}, Mg^{2+}, and HCO_3^- ions being the dominant constituents.

Groundwater facies Na+K+Ca-HCO_3 were identified at sample points PDG 1 and PDG 3, at an elevation of 645 masl and composed of tuff-breccia lithology (Apbt). High Na^+ concentrations in samples may indicate that they originated from the weathering of Sodium Feldspar or potassium feldspar. The result of the weathering of these rock minerals is the source of the presence of Na^+ cations and HCO_3 anions (Maria et al., 2021).

Groundwater facies Na+K+Ca-Cl were identified at sample point PDG 25, which has a reasonably high Cl- concentration (38.3 mg/L) due to the interaction of groundwater with sufficient rock. The observation point is situated in the oldest volcanic facies of the research area (Fbl), characterised by coarse lapilli lithology and located at a relatively low elevation on the sloping mountain (180 m a.s.l.), allowing Cl-ions to accumulate and representing meteoric water that has evolved during the relatively long circulation (Nsabimana and Li, 2023).

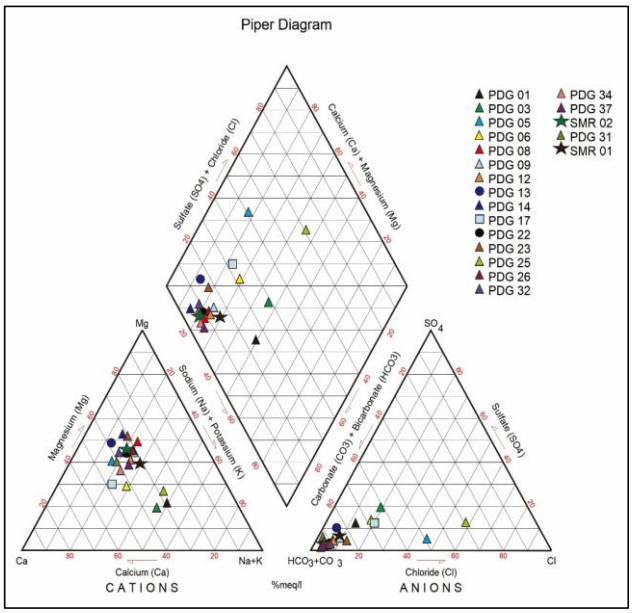

Fig 4. Plot Piper diagram of water samples in the study area

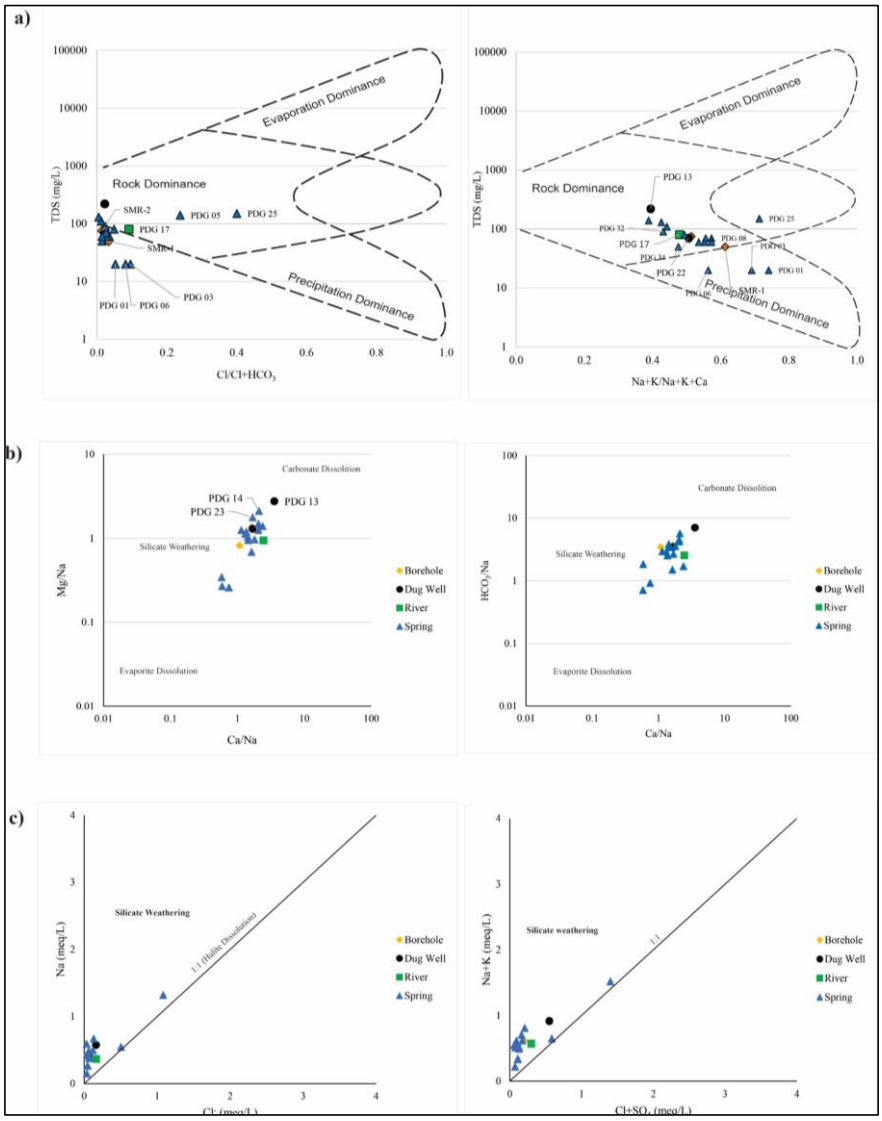

Fig 5. a) Plot major ions from the water sample to the Gibbs diagram in the study area b). Sample plot of the Gaillardet diagram using sodium normalised molar ratios in the dissolved phase. C). Scatter plot illustrating the correlation between major ions and hydrogeochemical processes (Na vs Cl; Na+K vs $Cl+SO_4$)

4.2 Groundwater Hydrochemical Processes

Groundwater hydrochemical processes control the mechanism of groundwater formation, which is influenced by the dominance of rainwater, rock weathering, crystallisation, or evaporation (Maria et al., 2021). A simple solution to studying the originating groundwater is to create a semi-logarithmic graph of the relationship between TDS and the Na+ ratio/(Na+ + Ca2+) and $Cl^-/(Cl^- + HCO3^-)$ (Gibbs 1970). the interpretation was performed using Gaillardet's diagram to confirm the water-rock interaction process in groundwater. The diagram classifies groundwater interaction processes as controlled by dissolution, silicate weathering, and carbonate dissolution (Gaillardet et al., 1999).

The ratio of TDS to the cation $(Na^+ + K^+)/(Na^+ + K^+ + Ca^{2+})$ indicates that rock weathering affects groundwater (Fig. 2). In contrast, the ratio of TDS to the anion (Cl/Cl+HCO3-) (Fig. 5a) suggests that rock weathering is dominant in the study area. The rock weathering-dominant type influences the chemical concentration of groundwater in the aquifer during the residence time (Ansari et al., 2019).

Based on the Gibbs diagram analysis, the samples that show the dominant influence of weathering are PDG 05, PDG 08, PDG 09, PDG 12, PDG 13, PDG 14, PDG 17, PDG 22, PDG 23, PDG 25, PDG 26, PDG 31, PDG 32, PDG 34, PDG 37, SMR-1, SMR-2 with TDS values ranging from 50 mg/L – 15 mg/L. These water samples are influenced by volcanic lithological weathering, which consists of several lithofacies, namely andesite lava (ALKsj), pyroclastic breccia-tuff grain supported facies (ALHbr), well-sorted lapilli tuff facies (PDct) and the old rough lapilli rock facies (Fbl).

According to Gaillardet's diagram in Fig. 3b, all samples fall within the silicate weathering section, indicating that the dissolution of silicate minerals has a significant influence on groundwater geochemistry in Cadasari, Banten.

Various methods can be employed to compare the ratios of major ions using bivariate plots, such as the Na vs Cl and Na + K vs Cl + SO_4 comparisons. Figure 5c illustrates the molar ratio between Na and Cl, where a Na/Cl ratio approaching 1 suggests that halite dissolution significantly contributes to the Na concentration in the groundwater. Conversely, if the ratio exceeds 1:1, it indicates that silicate weathering plays a dominant role in the geochemical process (Zhang et al., 2020). To further confirm the influence of silicate weathering, the ratio of Na + K to Cl + SO_4 was analysed (Fig. 5b). The groundwater samples plotted above the 1:1 line demonstrate that the silicate weathering process highly influences the groundwater's geochemistry.

4.3 The stable isotope composition of groundwater

Table 1 reports the isotopic composition of sample water in the study area. It shows borehole samples have an average isotope ratio of -7.0 ‰ for $\delta^{18}O$ and -41.7 ‰ for δ^2H, dug well samples have an average isotope ratio of -6.1 ‰ for $\delta^{18}O$ and -34.9 for δ^2H, and spring samples have an average isotope ratio of -6.7 ‰ for $\delta^{18}O$ and -39.3 for δ^2H.

The scatter plot shows the relationship between the δ2H and δ18O isotope values of the water samples and the meteoric water line. The solid line in Figure 6 is the local meteoric water line, and the dotted line is the global meteoric water line. PDG 32 is the only spring plotted right on the GMWL line, while PDG 25, PDG 31 and PDG 34 are springs plotted between GMWL and LMWL. PDG 12 is plotted directly on the LMWL; this indicates that the water on PDG 12 and PDG 17 is influenced by local rainfall. The depletion of $\delta^{18}O$, as in samples PDG-6 and SMR-1, may be due to different sources and associated with more distant rainwater flows to the surface. (Alçiçek et al., 2019; Bagheri et al., 2020; Hartanto et al., 2022)

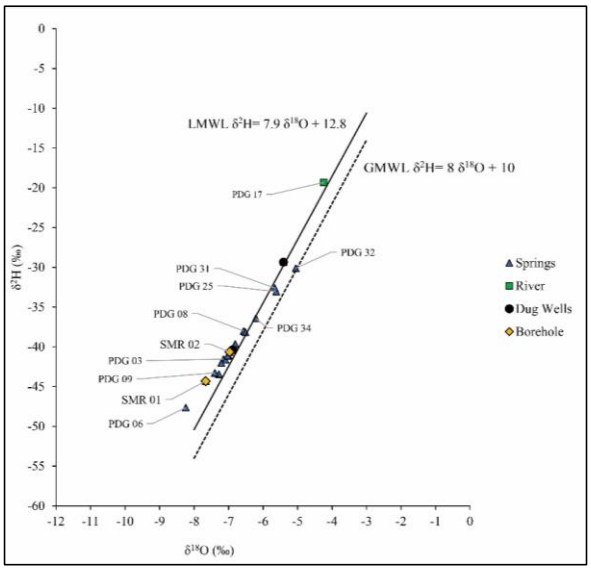

Figure 6. Scatter plot of $\delta^{18}O$ vs δ^2H of springs, rivers, and wells compared to Local meteoric water line (LMWL)(Hartanto et al., 2022) dan Global meteoric water line (GMWL)((Craig, 1961).

5. Conclusion

The interaction between groundwater and the minerals in the rock that forms the aquifer, along with changes in lithological units caused by several eruptions, leads to significant differences in the physical properties and chemical composition of the groundwater in Cadasari. Four distinct groundwater facies have been identified: Ca-HCO_3, Ca+Mg-HCO_3, Na+K-HCO_3, and Na+K+Ca-HCO_3. The Gibbs diagram indicates that water-rock interaction processes primarily control the variability of these groundwater facies in Cadasari. This was further confirmed by Gaillardet's diagram, which showed that all samples fall within the silicate weathering section, suggesting that silicate minerals play a crucial role in the geochemistry of the groundwater. Additionally, the isotopic composition of the groundwater samples indicates that the origin of the water in this area is meteoric.

Acknowledgements

The authors thank the Faculty of Geological Engineering, Padjadjaran University, and the Unpad team for their invaluable participation in this study.

References

Alam, B.Y.C.S., Itoi, R., Taguchi, S., Yamashiro, R., 2014. Spatial Variation in Groundwater Types in the Mt. Karang (West Java, Indonesia) Volcanic Aquifer System Based on Hydro-Chemical and Stable Isotope (?D and ?18O) Analysis. Mod. Appl. Sci. 8, p87. https://doi.org/10.5539/mas.v8n6p87

Alçiçek, H., Bülbül, A., Yavuzer, İ., Alçiçek, M.C., 2019. Hydrogeochemical and isotopic assessment and geothermometry applications in relation to the Karahayıt Geothermal Field (Denizli Basin, SW

Anatolia, Turkey). Hydrogeol. J. 27, 1791–1816. https://doi.org/10.1007/s10040-019-01927-y

Alfadli, M.K., Mardiana, U., Natasia, N., Mohammad, F., Mutaqin, D.Z., 2021. Resistivity Data Modeling for Subsurface Volcanostratigraphy Construction of Cibadak Sub-Watershed, Bogor, West Java, Indonesia. J. Geosci. Eng. Environ. Technol. 6, 74–80. https://doi.org/10.25299/jgeet.2021.6.2.2274

Ansari, Md.A., Deodhar, A., Kumar, U.S., 2019. Modeling of geochemical processes and multivariate statistical analysis for hydrochemical assessment of spring water of the Outer Himalaya, India. Environ. Earth Sci. 78, 665. https://doi.org/10.1007/s12665-019-8682-5

Bagheri, R., Karami, G.H., Jafari, H., Eggenkamp, H., Shamsi, A., 2020. Isotope hydrology and geothermometry of the thermal springs, Damavand volcanic region, Iran. J. Volcanol. Geotherm. Res. 389, 106745. https://doi.org/10.1016/j.jvolgeores.2019.106745

Bingar, B., 2024. warga-5-desa-di-kecamatan-cadasari-alami-krisis-air-bersih. bingar.id.

Craig, H., 1961. Isotopic variations in meteoric waters. Science 133, 1702–1703.

Dianardi, K., Jumhari, J., Hadian, M.S.D., Waliyana, T.Y., 2018. Characteristics of Groundwater on the Eastern Slope of Mount Ciremai, Kuningan Regency, West Java, Indonesia. J. Geosci. Eng. Environ. Technol. 3, 187. https://doi.org/10.24273/jgeet.2018.3.4.1606

Gaillardet, J., Dupre, B., Louvat, P., Allegre, C.J., 1999. from the chemistry of large rivers. Chem. Geol. 159, 3–30.

Gibbs, R.J., 1970. Mechanisms controlling world water chemistry. Science 170, 1088–1090.

Gong, Y., Liu, X., Ma, B., Qi, P., Li, Y., 2021. Using geochemistry and environmental tracers to study shallow unconfined aquifer recharge and mineralization processes in the Yinchuan Plain, arid Northwest China. Hydrol. Res. 52, 658–675. https://doi.org/10.2166/nh.2021.143

Hamed, Y., 2014. Stable isotope ratios in meteoric waters in El Kef Region, Northwestern Tunisia: implications for changes of moisture sources.

Hartanto, P., Alam, B.Y.C.S.S.S., Lubis, R.F., Ismawan, I., Iskandarsyah, T.Y.W.M., Sendjaja, Y.A., Hendarmawan, H., 2022. The application of hydrogeochemical and stable isotope data to decipher the origin and evolution of hot springs in the Rawadanau Basin, Indonesia. Geothermics 105, 102506. https://doi.org/10.1016/j.geothermics.2022.102506

He, X., Zhou, H., Wan, J., Guo, Y., Zhao, H., 2023. The effects of rainfall on groundwater hydrogeochemistry and chemical weathering. Environ. Sci. Pollut. Res. 30, 12152–12168.

Hendrayana, H., Harijoko, A., Riyanto, I.A., Nuha, A., Ruslisan, R., 2022. Groundwater Chemistry Characterization in the South and Southeast Merapi Volcano, Indonesia. Indones. J. Geogr. 55, 10. https://doi.org/10.22146/ijg.76433

Irawan, D.E., Puradimaja, D.J., Notosiswoyo, S., Soemintadiredja, P., 2009. Hydrogeochemistry of volcanic hydrogeology based on cluster analysis of Mount Ciremai, West Java, Indonesia. J. Hydrol. 376, 221–234. https://doi.org/10.1016/j.jhydrol.2009.07.033

Kottek, M., Grieser, J., Beck, C., Rudolf, B., Rubel, F., 2006. World Map of the Köppen-Geiger climate classification updated. Meteorol. Z. 15, 259–263. https://doi.org/10.1127/0941-2948/2006/0130

Laratmase, L., Kusumayudha, S.B., Harjanto, A., 2024. Geochemical Correlation of Volcanic Rocks and Groundwater Quality in the Todoko-Ranu Complex, Sahu District, West Halmahera, North Maluku, Indonesia. J. Geosci. Eng. Environ. Technol. 9, 341–348. https://doi.org/10.25299/jgeet.2024.9.3.15295

Listiawan, Y., Virgianty, A.S., Pramudyo, T., Iskandarsyah, T.Y.W.M., 2024. Groundwater Characteristics Analysis to Identify the Seawater Intrusion in Coastal Deep Aquifer System, Semarang, Central Java, Indonesia. J. Geosci. Eng. Environ. Technol. 9, 477–483. https://doi.org/10.25299/jgeet.2024.9.04.18561

Liu, J., Gao, Z., Feng, J., Wang, M., 2023. Identification of the hydrochemical features, genesis, water quality and potential health hazards of groundwater in Dawen River Basin, North China. Ecol. Indic. 149, 110175. https://doi.org/10.1016/j.ecolind.2023.110175

Liu, J., Gao, Z., Wang, M., Li, Y., Shi, M., Zhang, H., Ma, Y., 2019. Hydrochemical characteristics and possible controls in the groundwater of the Yarlung Zangbo River Valley, China. Environ. Earth Sci. 78, 76. https://doi.org/10.1007/s12665-019-8101-y

Liu, Y., Yamanaka, T., 2012. Tracing groundwater recharge sources in a mountain–plain transitional area using stable isotopes and hydrochemistry. J. Hydrol. 464, 116–126.

Mardiana, 2024. Setiap Tahun Kesulitan Air Bersih, Warga 4 Kampung di Cadasari Pandeglang Berharap Solusi. www.satelitnews.com.

Maria, R.M., Satrio, S., Iskandarsyah, T.Y.W.M., Suganda, B.R., Delinom, R.M., Marganingrum, D., Purwoko, W., Sukmayadi, D., Hendarmawan, H., 2021. Groundwater Recharge Area Based on Hydrochemical and Environmental Isotopes Analysis in the South Bandung Volcanic Area. Indones. J. Chem. 21, 609. https://doi.org/10.22146/ijc.58633

Nsabimana, A., Li, P., 2023. Hydrogeochemical characterization and appraisal of groundwater quality for industrial purpose using a novel industrial water quality index (IndWQI) in the Guanzhong Basin, China. Geochemistry 83, 125922. https://doi.org/10.1016/j.chemer.2022.125922

Oliveira, M.S., Neves, M.A., Caxito, F.A., Moreira, R.M., 2022. 18O, 2H, and ^{3}H isotopic data for understanding groundwater recharge and circulation systems in crystalline rocks terrain of Southeastern Brazil. J. South Am. Earth Sci. 116, 103794.

Piper, A.M., 1944. A graphic procedure in the geochemical interpretation of water-analyses. Eos Trans. Am. Geophys. Union 25, 914–928.

Razi, M.H., Wilopo, W., Putra, D.P.E., 2024. Specifying groundwater recharge zones through hydrogeochemical and isotopic analyses in a multilayer volcanic aquifer: a case study in the Yogyakarta-Sleman Groundwater Basin,

Indonesia. Hydrogeol. J. 32, 2167–2183. https://doi.org/10.1007/s10040-024-02849-0
Rusmana, E., 1991. Geological map of the Serang Sheet Region, Java.
Suganda, B.R., Yusuf, W., Barkah, M.N., Sunarie, C.Y., Hadian, M.S.D., 2021. Shallow Aquifer Groundwater Facies At Multiple Landuse Sites In Manglayang Volcanic Area, Jatinangor And Surroundings, Indonesia. J. Geosci. Eng. Environ. Technol. 6, 120–126. https://doi.org/10.25299/jgeet.2021.6.2.3315
Toulier, A., Baud, B., De Montety, V., Lachassagne, P., Leonardi, V., Pistre, S., Dautria, J.-M., Hendrayana, H., Miftakhul Fajar, M.H., Satrya Muhammad, A., Beon, O., Jourde, H., 2019. Multidisciplinary study with quantitative analysis of isotopic data for the assessment of recharge and functioning of volcanic aquifers: Case of Bromo-Tengger volcano, Indonesia. J. Hydrol. Reg. Stud. 26, 100634. https://doi.org/10.1016/j.ejrh.2019.100634
Zhang, B., Zhao, D., Zhou, P., Qu, S., Liao, F., Wang, G., 2020. Hydrochemical Characteristics of Groundwater and Dominant Water–Rock Interactions in the Delingha Area, Qaidam Basin, Northwest China. Water 12, 836. https://doi.org/10.3390/w12030836